THE JOURNAL OF PHYSICAL CHEMISTRY C

Article

pubs.acs.org/JPCC

Utilizing the Gate-Opening Mechanism in ZIF-7 for Adsorption Discrimination between N_2O and CO_2

De-Li Chen,[†] Ningwei Wang,[†] Fang-Fang Wang,[†] Jianwu Xie,[†] Yijun Zhong,[†] Weidong Zhu,*[,†] J. Karl Johnson,[‡,§] and Rajamani Krishna*[,∥]

[†]Key Laboratory of the Ministry of Education for Advanced Catalysis Materials, Institute of Physical Chemistry, Zhejiang Normal University, 321004 Jinhua, China

[‡]Department of Chemical and Petroleum Engineering, University of Pittsburgh, Pittsburgh, Pennsylvania 15261, United States

[§]National Energy Technology Laboratory, Pittsburgh, Pennsylvania 15236, United States

[∥]Van't Hoff Institute for Molecular Science, University of Amsterdam, Science Park 904, 1098 XH Amsterdam, The Netherlands

Supporting Information

ABSTRACT: N_2O is a greenhouse gas with tremendous global warming potential, and more importantly it also causes ozone depletion; thus, the separation of N_2O from industrial processes has gained significant attention. We have demonstrated that N_2O can be selectively separated from CO_2 using the zeolite imidazolate framework ZIF-7. The adsorption/desorption isotherms of both N_2O and CO_2 in ZIF-7 indicate the gate-opening mechanism of this material, and surprisingly, the threshold pressure for the gate opening with N_2O is lower than that with CO_2. Theoretical calculations indicate that both gas−host and gas−gas interaction energies for N_2O are more favorable than those for CO_2, giving rise to the difference in the threshold pressure between N_2O and CO_2 in ZIF-7. Breakthrough experiments for N_2O/CO_2 mixtures confirm that ZIF-7 is capable of separating N_2O and CO_2 mixtures under the optimized conditions, in reasonable agreement with simulation results, making it a promising material for industrial applications.

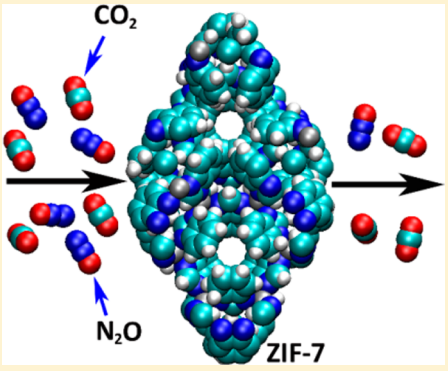

1. INTRODUCTION

Nitrous oxide (N_2O) has recently attracted significant attention due to its increasing negative impacts to the environment, not only because of its greenhouse effect but also for the ozone layer depletion. Although N_2O is not a major contributor to global warming (~6%),[1] it was reported that N_2O has about 300 times the global warming potential of the most common greenhouse gas CO_2, due to its long lifetime of approximately 120 years in the atmosphere.[2] On the other hand, N_2O is the major source of nitrogen oxides in the stratosphere and thus the main naturally occurring regulator of stratospheric ozone.[3,4] It was reported that about 40% of total N_2O emissions come from human activities, arising from agriculture, transportation, and industry activities.[5]

Industrial N_2O emissions are generated as a byproduct of adipic acid and nitric acid production.[6] Two ways are considered to be alternatives to dispose of N_2O. One is the conversion of N_2O with low concentration, including direct decomposition and selective catalytic reduction, into environmentally friendly N_2.[7] The other is the use of high-concentration N_2O as an active oxygen donor, e.g., one-step oxidation of benzene to phenol with N_2O.[8] However, the catalytic decomposition of N_2O typically occurs at high temperatures and cannot recover N_2O as a valuable intermediate for the production of other fine chemicals.[6] Thus, development of an efficient and economic technology such as physisorption to capture or concentrate N_2O and then to use it as the oxidant to produce important fine chemicals such as phenol would be highly desired.[9] In the tail gases of adipic acid and nitric acid production processes, N_2O shares many structural and physical similarities with CO_2 including molecular size and quadrupole moment,[10] making it a great challenge to find suitable adsorptive materials for the separation of N_2O/CO_2 mixtures. The major difference between these two gases is that N_2O has a small dipole moment of 0.167 D while for CO_2 the dipole moment is zero due to symmetry.[11]

In the past decade, different materials have been investigated for the purpose of separating N_2O/CO_2 mixtures.[12−15] Recently, ionic liquids were proposed for separation of N_2O. However, the first experimental measurement on the solubility of N_2O using ionic liquid was reported to be essentially the same as CO_2.[12] Interestingly, Shiflett et al.[13] found that with ionic liquids the selectivity for N_2O over CO_2 could reach 1.4−1.5, based on calculations using a ternary equation of state model. Moreover, van der Bergh et al.[14] reported that a DD3R zeolite membrane could not distinguish these binary gas

Received: June 7, 2014
Revised: July 14, 2014
Published: July 14, 2014

   dx.doi.org/10.1021/jp5056733 | J. Phys. Chem. C 2014, 118, 17831−17837

mixtures. Metal-exchanged zeolites were used to concentrate gaseous N_2O, leading to a concentration of 5 vol % that is still insufficient to meet practical requirements.[15] Metal−organic frameworks (MOFs) and zeolitic imidazolate frameworks (ZIFs) offer great flexibility for tuning the adsorbate−adsorbent interaction through the huge combination of potential functional groups available. Therefore, MOFs and ZIFs offer the potential to selectively capture N_2O and produce a concentrated stream of N_2O. The zeolitic imidazolate framework ZIF-7 is a prototypical ZIF material reported by Yaghi et al.,[16] having a sodalite topology with a SOD cage (d = 4.31 Å) and a six-membered-ring opening window (d = 3.0 Å). ZIFs are very attractive for different separation applications because of their intrinsic properties such as high stability and wide topological variety. ZIF-7 exhibits a dynamic framework upon external stimuli such as pressure and temperature, known as gate-opening effects.[17,18] Consequently, adsorbing molecules with kinetic diameters larger than 3.0 Å were found to penetrate the narrow apertures in ZIF-7. More interestingly, the framework flexibility as found in many flexible MOFs has been utilized to separate gas molecules with similar sizes.[11,17−19] In ZIF-7, it was explained that the benzimidazole linkers are able to rotate over a certain angle making the pore size increased and thus allowing molecules larger than 3.0 Å to enter the main cavities.[17,20] This phenomenon is somewhat different from the breathing effects found in some MOFs.[21,22]

In this study, we aim to utilizing the gate-opening mechanism of ZIF-7 for discriminating two linear gas molecules, i.e., N_2O and CO_2. The mechanism will be illustrated with combined experimental and theoretical method. The state-of-the-art periodic density functional theory (DFT) with the inclusion of dispersion correction was employed for calculations to overcome the inherent limitations of cluster model based calculations, where the confinement effect was not well reproduced.[18]

2. METHODS

2.1. Synthesis and Characterization of ZIF-7. The synthesis of ZIF-7 crystals was carried out according to the procedure reported by Gücüyener et al.[17] A solid mixture of $Zn(NO_3)_2{\cdot}6H_2O$ (0.598 g) and benzimidazole (0.479 g) was dissolved in 75 mL of *N*,*N*-dimethylformamide (DMF) and stirred for a few minutes at room temperature. The prepared solution was then transferred to a Teflon-lined stainless steel autoclave, and the synthesis was carried out without agitation in an oven at 403 K for 48 h. The solid product was then filtered, washed with methanol, and dried at 373 K for one night. The obtained ZIF-7 sample was confirmed by powdered X-ray diffraction (XRD) patterns performed on a Philips PW3040/60 diffractometer using Cu Kα radiation (λ = 0.1541 nm) in a scanning range of 5−50° with a step size of 0.033°. The XRD pattern and scanning electron microscopy (SEM) images of the synthesized ZIF-7 are shown in Supporting Information Figures S1 and S2, respectively.

2.2. Isotherm Measurement and Fitting. The single-component adsorption/desorption isotherms of N_2O and CO_2 on the pellet sample, prepared from the synthesized sample pressed at 1 MPa and then crushed into particles with sizes from 0.38 to 0.55 mm in diameter, were measured by a Micromeritics ASAP 2020 instrument. The sample cell was loaded with ca. 500 mg of the adsorbent. After the adsorbent was outgassed under vacuum at 423 K for 10 h in order to remove any adsorbed impurities, prior to the adsorption/desorption measurements, the adsorption/desorption runs were carried out at 298 K.

The measured adsorption/desorption isotherms of pure gases N_2O and CO_2 were fitted by the dual-site Langmuir−Freundlich (DLF) isotherm model:

$$q = q_{A,sat}\frac{b_A p^{\nu_A}}{1 + b_A p^{\nu_A}} + q_{B,sat}\frac{b_B p^{\nu_B}}{1 + b_B p^{\nu_B}} \quad (1)$$

where q is the adsorbed amount, p is the pressure, $q_{A,sat}$ and $q_{B,sat}$ represent the saturation adsorption capacities at two different adsorption sites A and B, respectively, and b_A and b_B are the equilibrium constants at adsorption sites A and B, respectively. All fitted parameters are summarized in Supporting Information Table S1. The fitted isotherms based on the DLF model agree well with the measured adsorption/desorption isotherms (Supporting Information Figures S3 and S4). Based on the fitted isotherms, the ideal adsorbed solution theory (IAST) was then applied to predict the adsorption selectivity (see Supporting Information Figure S5) of N_2O/CO_2.

2.3. Quantum Chemical Calculations. All of our density functional theory calculations were performed in Vienna *ab initio* simulation package.[23−26] The van de Waals density functional (vdW-DF), specifically using the vdW-DF2,[27,28] was used to accurately reproduce the vdW energy between the gas molecules (N_2O and CO_2) and framework. The Brillouin zone was sampled using Monkhorst−Pack grids[29] of 1 × 1 × 1 for all of the calculations, where a planewave energy cutoff of 400 eV was employed. In this study the experimentally measured unit cell (a = b = 22.989 Å; c = 15.763 Å)[30] was fixed while the atoms on the framework of ZIF-7 were fully relaxed using vdW-DF2. During the structural optimization of adsorbates/ZIF-7, all of the atoms were allowed to relax until the force on each ion was less than 0.005 eV/Å.

For evaluating the intermolecular interaction of $N_2O{\cdots}N_2O$ (or $CO_2{\cdots}CO_2$) linear configuration, the second-order Møller−Plesset perturbation theory MP2 method[31] together with basis set of aug-cc-pVTZ was employed for structural optimizations and then the optimized structures (see Supporting Information Figure S7) were used for single-point calculations using explicitly correlated coupled cluster singles and doubles with perturbative triples method [CCSD(T)-F12a][32,33] implemented in Molpro program.[34] The DFT-SAPT method[35] was used for decomposition of the interaction energies between CO_2 (or N_2O) molecules.

2.4. Breakthrough Experiments and Simulations. The setup consists of three sections: a gas mixing and flow control section, a breakthrough column, and an analysis section. A flowsheet diagram of the setup is shown in Supporting Information Figure S8. The breakthrough column was installed inside the ceramic oven, which was located inside the convection oven. The external diameter of the column was 6.35 mm with a length of 15 cm, and the inner diameter was 4.65 mm. A 0.89 g amount of the ZIF-7 pellet sample was packed into the column. The quartz wool was placed at the top and bottom of the column. Prior to the breakthrough experiments, the adsorbent was outgassed overnight at 473 K with a He flow rate of 20 mL(STP)/min. The mass spectrometer (Pfeiffer Vacuum OmniStar GSD 320) in the analysis section was used to monitor the component concentrations continuously. However, for N_2O/CO_2 mixtures, most of the intense m/e peaks overlap and thus the composition cannot be identified by the

dx.doi.org/10.1021/jp5056733 | J. Phys. Chem. C 2014, 118, 17831−17837

mass spectrometer. In order to determine the breakthrough and desorption profiles of the mixture compositions, the isotope gas $^{13}CO_2$, provided by Beijing Mingnike Analytical Instrument Center (^{13}C > 99% and ^{18}O < 1%), was used. The N_2O was supplied by Beijing Praxair Application Gas Co., Ltd. (>99.99%). The breakthrough experiments were performed at a total pressure of 200 kPa and 298 K by switching the flow to the column from He to N_2O and $^{13}CO_2$ in He. After the breakthrough curves reached the equilibrium, the mixture feed flow of N_2O and $^{13}CO_2$ in He was switched back to the He flow with a rate of 20 mL(STP)/min and the desorption curves were recorded.

Transient breakthroughs are influenced by both mixture adsorption equilibrium and intracrystalline diffusion. In order to determine the extent of the relative importance of adsorption and diffusion in determining the separation performance, we perform transient breakthrough simulations and compare these with experimental data. The details of the simulation methodology used to perform transient breakthrough calculations are given in the Supporting Information (SI).

3. RESULTS AND DISCUSSION

We report here an unexpected phenomenon that ZIF-7 is able to separate N_2O/CO_2 mixtures, although the two molecules have almost the same size. The hysteresis adsorption/desorption isotherms of CO_2 in ZIF-7 as shown in Figure 1

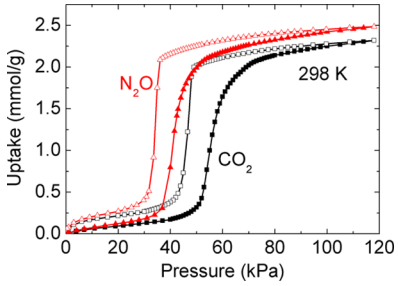

Figure 1. Measured adsorption (desorption) isotherms of N_2O and CO_2 in ZIF-7 at 298 K, presented as filled (open) triangles and filled (open) squares, respectively.

are similar to those observed for light hydrocarbons in ZIF-7.[17] The measured CO_2 loading at 100 kPa is about 2.25 mmol/g, in excellent agreement with the data reported by Aguado et al.[36] A step region exists in the CO_2 isotherm, where the CO_2 uptake increases sharply from about 0.32 to 1.64 mmol/g in a narrow pressure range from 50 to 60 kPa. We attribute this step region to a process of the opening of the six-membered-ring windows in ZIF-7, where CO_2 molecules rapidly fill the main cavities. The N_2O isotherm shows three regions similar to CO_2, but with a step region at a relatively lower pressure, where the N_2O uptake strongly increases from about 0.30 to 1.73 mmol/g over a narrow pressure range from 35 to 45 kPa. Obviously, the gate-opening pressure (also denoted as threshold pressure) of about 35 kPa for N_2O is lower than 50 kPa for CO_2. IAST[37] was employed to estimate the separation performance of N_2O/CO_2 mixtures, based on the fitted isotherms using the dual-site Langmuir–Freundlich model (see SI for details), and the calculations indicate the separation selectivity of N_2O over CO_2 ranges from 1.4 to 1.7 (SI Figure S5) for pressures up to 100 kPa. The accuracy of IAST calculations has been established in section VI of the SI on the basis of mixture breakthrough experiments to be discussed below.

Microporous materials have been widely used for the molecular-sieving separation of binary gas mixtures, where two different molecules have different sizes.[38] However, N_2O and CO_2 have the same kinetic diameter of 3.3 Å,[10] and thus the driving force of different threshold pressures in ZIF-7 remains unclear. The gas–host interaction between gas molecules and ZIF-7 framework mainly consists of electrostatic energy and van der Waals (vdW) energy, and thus accurate first-principles calculations are required to obtain reliable gas–host interaction energies. The van der Waals density functional has been successfully used to reproduce weak vdW energy in many different systems,[39−41] and thus this method was employed here to compute the adsorption energies of both N_2O and CO_2 at various sites in the periodic ZIF-7 structure. We scanned the potential energy curves of both CO_2 and N_2O passing through the pore along the z-axis, where each configuration was allowed to move on a window perpendicular to the z-axis during the structural optimization. Our calculations show that the neck (denoted as pore-A in Figure 2a,c) along the z-axis is formed by three benzene rings, and the

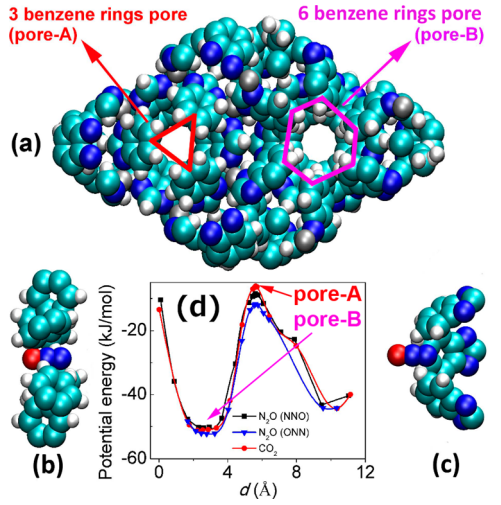

Figure 2. (a) The (110) surface of the optimized ZIF-7 crystal structure and two different types of pores along the z-axis, where the pore-A (red) and pore-B (purple) represent three- and six-benzene-ring pores, respectively; the configurations of N_2O (with NNO orientation) at (b) pore-B and (c) pore-A, where only a few atoms surrounding the N_2O molecule are shown for clarity; (d) vdW-DF2 calculated potential energy curves of CO_2 and N_2O (with orientations of NNO and ONN) passing through the channel along the z-axis as a function of distance d along the z-axis.

adsorption energy of CO_2 at this site is −6.1 kJ/mol. N_2O has two different orientations along the z-axis, i.e., NNO or ONN, having potential energies at the neck sites of −8.5 and −11.8 kJ/mol, respectively. Thus, either orientation of N_2O has a more favorable adsorption energy than CO_2 at the narrowest site in ZIF-7. This is consistent with the smaller threshold pressure for N_2O. The pore-B site (Figure 2a,b), formed with six benzene rings, is also located along the z-axis and is located about 3.0 Å away from the pore-A site in the z-direction, where the potential energies for CO_2, NNO, and ONN are −51.0, −52.2, and −50.4 kJ/mol, respectively. These calculations indicate that N_2O is bound more strongly than CO_2 in pore-A, while in the larger pore-B the binding energies are almost the

dx.doi.org/10.1021/jp5056733 | J. Phys. Chem. C 2014, 118, 17831−17837

same. This is consistent with the selectivity for N_2O over CO_2 computed from IAST. It would be worthwhile to note that the adsorption of either N_2O or CO_2 at the pore-A site leads to an opening of the gate with size from 4.8 to 5.7 Å (see SI Figure S6), while pore-B size is almost unchanged upon the adsorption of either N_2O or CO_2.

In addition to gas−host interactions, it is well-known that the gas−gas intermolecular interaction may enhance the adsorption strength.[42,43] Therefore, we also evaluate the intermolecular interaction of the gases to see how these forces may affect the adsorption in ZIF-7. Considering the confinement effect due to the narrow pores in ZIF-7, it is reasonable to evaluate the intermolecular interaction by calculating the molecular dimer with linear configuration. We performed structural optimization by doing MP2/aug-cc-pVTZ calculations in vacuum, based on which we obtained the interaction energy with CCSD(T)-F12a/aug-cc-pVTZ. The results show that the NNO···ONN (NNO···NNO) linear configuration has an attractive interaction energy of −1.3 (−0.8) kJ/mol; however, the OCO···OCO linear configuration has a much less attractive interaction energy of −0.1 kJ/mol. Decomposition of the interaction energies (see SI Table S2) using the DFT-SAPT method explains the origin of these differences. The two symmetric configurations OCO···OCO and NNO···ONN have almost the same dispersion energies, but the CO_2 dimer has more repulsive electrostatic and exchange energies than the N_2O dimer by about 0.6 and 0.7 kJ/mol, respectively. The NNO···NNO orientation has slightly more favorable dispersion energy, but much less favorable (more repulsive) exchange energies compared with the NNO···ONN configuration (SI Table S2), resulting in a slightly larger intermolecular distance (SI Figure S7). We note that the NNO···NNO orientation has a favorable dipole−dipole interaction but that the overall electrostatic interaction is still repulsive because the repulsive quadrupole−quadrupole term dominates the electrostatic interaction at this distance (see SI for details). Hence, the larger binding energy for the NNO···ONN dimer is mainly due to the less repulsive exchange energy. Hence, gas−gas N_2O interactions contribute an additional ∼1 kJ/mol to the adsorption energy of N_2O, while CO_2 intermolecular interactions are negligible in the narrow pores of ZIF-7. Note that the T-shape CO_2 intermolecular interaction enhances the adsorption energy of CO_2 in some nanoporous materials;[42,43] however, the narrow pores of ZIF-7 cannot accommodate the T-shape CO_2 dimer. In summary, the stronger N_2O adsorption energy and more favorable gas−gas interaction lead to its lower threshold pressure.

We performed breakthrough experiments to assess the practical application of ZIF-7 in separating the gas mixtures. The experiments were conducted using $N_2O/CO_2/He$ gas mixtures. The flow rate of He was held constant at 4 mL/min and the total pressure of the ternary gas mixture was maintained at 200 kPa for all three breakthrough experiments. The partial pressures of N_2O and CO_2 were varied from 20 to 50 and 90 kPa at the inlet of the column by altering the molar ratios of the $N_2O/CO_2/He$ mixtures from 1:1:8 (noted as exp-1) to 1:1:2 (exp-2) and 4.5:4.5:1 (exp-3), respectively. In exp-1, shown in Figure 3, the breakthroughs of both gases are obtained at a time of about 200 s and the mole fraction rapidly increases to a constant value of 0.1, with CO_2 being slightly faster than N_2O. We ascribe this process to the adsorption of the gas mixture on the surfaces of ZIF-7 pellets as well as in the spaces between them, since a partial pressure of 20 kPa is

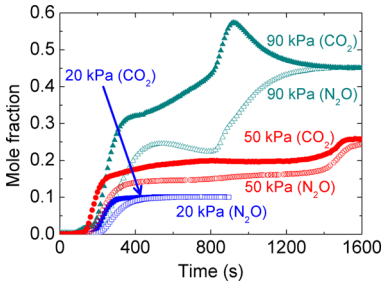

Figure 3. Measured mole fractions of N_2O (open symbols) and CO_2 (filled symbols) in the outlet of the column from the three breakthrough experiments at 298 K as a function of time, where N_2O and CO_2 partial pressures in the inlet of the column are 20, 50, and 90 kPa, respectively.

smaller than the threshold pressure of either N_2O or CO_2 and thus the gates of ZIF-7 are closed during the whole process. With the partial pressures of both N_2O and CO_2 set to 50 kPa in exp-2, some interesting features are obtained. As shown in Figure 3, the curves for the first stage (0−300 s) of exp-2 are very similar to the curves of exp-1 before reaching the plateau. The difference is that the first stage in exp-2 ends with mole fractions of 0.16 (CO_2) and 0.14 (N_2O), smaller than 0.25 at equilibrium, which could be explained as follows: with an inlet N_2O partial pressure of 50 kPa, the gates of ZIF-7 are opened, allowing N_2O molecules to enter the main cavity, while the partial pressure of CO_2 keeps increasing until the higher threshold pressure (>50 kPa) of CO_2 is reached. Therefore, the second stage consists of steady curves, where the mole fraction in the outlet of the column slowly increases until the main cavities are fully filled with N_2O and CO_2 but the competing adsorption seems to be favorable for N_2O, resulting in a lower concentration of N_2O in the outlet of the column. Afterward, in the third stage, the mole fractions of both species sharply increase again, where the main cavities of ZIF-7 are almost saturated. We note that there is a roll-up curve for CO_2 in the third stage above 0.25, which is not surprising since it corresponds to a mole fraction of N_2O smaller than 0.25. At the end of this process, both N_2O and CO_2 reach a steady flow rate in the outlet of the column. In exp-3, with partial pressures for both N_2O and CO_2 at the inlet of the column fixed to 90 kPa (Figure 3), a similar three-stage process (compared to exp-2) is obtained, accompanied by some differences in the second and the third stages. Interestingly, in the second stage, the measured CO_2 mole fraction keeps increasing in the outlet of column while N_2O mole fraction gradually decreases, indicating more N_2O molecules are adsorbed in the column, which could be explained as the competing adsorption of N_2O over CO_2. When the adsorption of N_2O in the column is close to a maximum loading at the end of the second stage, the mole fraction of N_2O in the outlet of the column rapidly increases in the third stage until an equilibrium value (0.45) is reached, while a steep roll-up curve is found for CO_2 with the largest mole fraction of 0.55 in the third stage and then drops rapidly to 0.45 at equilibrium. In contrast to exp-2, the difference in the adsorbed amount between N_2O and CO_2 is larger in exp-3, indicating the larger partial pressure (over the threshold pressure) facilitates the gas mixture separation.

The above breakthrough experiments have important implications. We only observe significant differences in adsorption between N_2O and CO_2 when the partial pressure of the adsorbing component is larger than its threshold

dx.doi.org/10.1021/jp5056733 | J. Phys. Chem. C 2014, 118, 17831−17837

pressure. Otherwise, both gases are not able to enter the main cavity of ZIF-7 and thus essentially no difference in breakthrough is obtained. The gate-opening effect is evidenced from the breakthrough experiments where the higher partial pressures of the adsorbing gases give rise to higher separation factors. To the best of our knowledge, none of the MOFs and ZIFs synthesized to date has been reported to be capable of efficiently separating N_2O/CO_2 gas mixtures. Therefore, our breakthrough experiments on ZIF-7 showing the capability of separating N_2O from CO_2 is a *breakthrough* to this field, opening the door to selective separation of N_2O/CO_2 gas mixtures with an appreciable separation efficiency.

From a practical point of view, it is also very important for the regeneration process to have high efficiency and low energy cost. To understand how the ZIF-7 performs on the desorption process of the adsorbed components from the ZIF-7 bed, we carried out the desorption experiments from exp-1, exp-2, and exp-3, by supplying a stream of pure He to flush the column at a flow rate of 20 mL/min. In all of the three cases, the desorption curves (see SI Figure S9) show that the concentration of the weaker adsorbed CO_2 declines faster than that of N_2O, and the separation selectivity is similar to that observed for the adsorption process.

Breakthrough simulations have recently been proposed to be a valuable tool for screening MOFs with reasonable accuracy.[44−46] Even though the accuracy of IAST has not been established for mixture adsorption under conditions of gate opening previously, we found that there is a reasonable agreement of adsorption loadings between experiments and IAST predicted data (see section VI of the SI for details). We use the IAST mixture isotherms to simulate breakthrough curves for the gas mixtures by assuming a plug flow through the adsorbent bed and solving a set of partial differential equations. The influence of intracrystalline diffusion is also evaluated in our simulation to see how it affects the results. We have simulated the three sets of the breakthrough curves discussed above, with and without the consideration of intracrystalline diffusion. Taking exp-2 as an example (Figure 4), we observe that breakthrough simulations are able to predict the correct breakthrough times for N_2O and CO_2. The agreement of the gas-phase compositions obtained from simulations with those determined from experiments is somewhat less accurate. We also notice that the consideration of intracrystalline diffusion does not significantly affect the simulation, indicating that the separation is dominated by adsorption thermodynamics. However, for the chosen partial pressure of 90 kPa, the agreement between simulation and experiment is improved by taking intracrystalline diffusion into account (see SI Figure S11). Based on the breakthrough simulations, we computed the CO_2/N_2O and N_2O/CO_2 ratios in the outlet column for adsorption and desorption cycles, respectively, where both ratios lie between 1.5 and 7.5 depending on different time intervals and different partial pressures (see SI Figure S12), larger than the estimated separation factor from IAST (1.4−1.7). This confirms the potential application of using ZIF-7 for N_2O/CO_2 separation. It is also worthwhile to mention that utilizing the gate-opening mechanism of ZIF-7 N_2O could be efficiently separated from other gases such as N_2. With the reported N_2 isotherm data in ZIF-7 by Reyes et al.,[47] we simulated a ternary 1:1:2 $N_2O/CO_2/N_2$ mixture in a fixed bed operating at a total pressure of 100 kPa and the breakthrough simulations (see SI Figure S15) clearly confirm the high separation selectivity of both N_2O/N_2 and CO_2/N_2 mixtures.

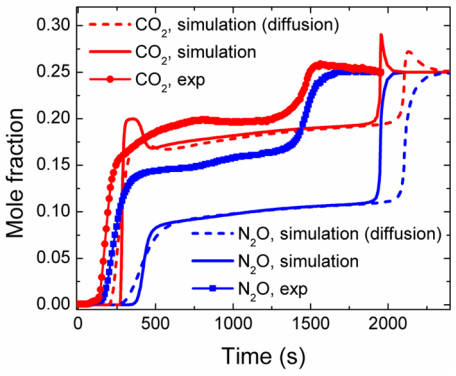

Figure 4. Comparison of the breakthrough simulation and experiment (exp-2), where the partial pressures of CO_2 and N_2O in the inlet column are 50 kPa. The symbols represent experimental data; solid lines and dashed lines are for simulation data without and with the consideration of intracrystalline diffusion, respectively.

4. CONCLUSION

The combined experimental and theoretical methods including isotherm measurements, transient breakthrough experiments and simulations, as well as stat-of-the-art quantum chemical method, were used to study the adsorption and separation performance of two linear molecules, N_2O and CO_2, with the same molecular sizes and very similar physical properties in ZIF-7. The gate-opening mechanism of ZIF-7 is not only evidenced by the isotherm and breakthrough measurements but also confirmed by vdW-DF2 calculations. The experimental observations on the different gate-opening pressures between N_2O and CO_2 were explained as the different adsorption energies at the neck sites in ZIF-7 via quantum chemical calculations using the vdW-DF2 method. The measured breakthrough curves were reasonably modeled by the transient breakthrough simulation methodology employed in this study. We found that the gate-opening mechanism of ZIF-7 can potentially be utilized to separate N_2O/CO_2 gas mixtures with an appreciable efficiency. The combined experimental and theoretical investigations confirm the potential application of this material in industry for separating N_2O/CO_2 mixtures, which might open the door of an efficient adsorptive separation for N_2O. It is speculated that utilizing the gate-opening mechanism of ZIF-7 we would be able to separate N_2O from other nitrogen oxides, such as NO (larger dipole moment) and NO_2 (larger kinetic diameter), both of which are generated from nitric acid production processes. The intriguing results in this study make ZIF-7 a very promising material for discriminating N_2O from other gases.

■ ASSOCIATED CONTENT

Supporting Information

Experimental details for synthesis, characterization, XRD data, breakthrough experiments, simulation details for breakthrough simulations and quantum chemical calculations, comparisons of breakthrough experiments and simulations at the different conditions, captions describing the accompanying videos, and video animations of the transient breakthrough at 298 K. This material is available free of charge via the Internet at http://pubs.acs.org.

dx.doi.org/10.1021/jp5056733 | J. Phys. Chem. C 2014, 118, 17831−17837

AUTHOR INFORMATION

Corresponding Authors

*E-mail: weidongzhu@zjnu.cn.
*E-mail: r.krishna@contact.uva.nl.

Notes

The authors declare no competing financial interest.

ACKNOWLEDGMENTS

W.Z. and D.-L.C. gratefully acknowledge the support from the National Natural Science Foundation of China (Grants 21036006 and 21303165). Theoretical calculations were performed at the University of Pittsburgh Center for Simulation and Modeling.

REFERENCES

(1) Houghton, J. T., Callander, B. A., Verney, S. K., Eds.; *Climate change 1992: The supplementary Report to the IPCC Scientific Assessment*; IPCC: Cambridge, U.K., 1992.

(2) http://epa.gov/climatechange/ghgemissions/gases/n2o.html.

(3) Ravishankara, A. R.; Daniel, J. S.; Portmann, R. W. Nitrous Oxide (N_2O): The Dominant Ozone-Depleting Substance Emitted in the 21st Century. *Science* **2009**, *326*, 123−125.

(4) Pérez-Ramírez, J.; Kapteijn, F.; Schöffel, K.; Moulijn, J. A. Formation and Control of N_2O in Nitric Acid Production: Where Do We Stand Today? *Appl. Catal., B* **2003**, *44*, 117−151.

(5) EPA. *Methane and Nitrous Oxide Emissions from Natural Sources*. . U.S. Environmental Protection Agency: Washington, DC, USA, 2010.

(6) Groen, J. C.; Pérez-Ramírez, J.; Zhu, W. D. Adsorption of Nitrous Oxide on Silicalite-1. *J. Chem. Eng. Data* **2002**, *47*, 587−589.

(7) Xiao, Q.; Yang, F. F.; Zhuang, J.; Qiu, G. P.; Zhong, Y. J.; Zhu, W. D. Facile Synthesis of Uniform FeZSM-5 Crystal with Controlled Size and Their Application to N_2O Decomposition. *Microporous Mesoporous Mater.* **2013**, *167*, 38−43.

(8) Zhang, F. M.; Chen, X.; Zhuang, J.; Xiao, Q.; Zhong, Y. J.; Zhu, W. D. Direct Oxidation of Benzene to Phenol by N_2O over Meso-Fe-ZSM-5 Catalysts Obtained via Alkaline Post-Treatment. *Catal. Sci. Technol.* **2011**, *1*, 1250−1255.

(9) Thallapally, P. K.; McGrail, B. P.; Atwood, J. L. Sorption of Nitrogen Oxides in a Nonporous Crystal. *Chem. Commun.(Cambridge, U. K.)* **2007**, 1521−1523.

(10) Eguchi, R.; Uchida, S.; Mizuno, N. Inverse and High CO_2/C_2H_2 Sorption Selectivity in Flexible Organic-Inorganic Ionic Crystals. *Angew. Chem., Int. Ed.* **2012**, *51*, 1635−1639.

(11) Nelson, R. D., Jr.; Lide, D. R., Jr.; Maryott, A. A. *Selected Values of Electric Dipole Moments for Molecules in the Gas Phase, NSRDS-NBS10; National Standard Reference Data System-National Bureau of Standards*: Washington, DC, USA,1967.

(12) Anthony, J. L.; Anderson, J. L.; Maginn, E. J.; Brennecke, J. F. Anion Effects on Gas Solubility in Ionic Liquids. *J. Phys. Chem. B* **2005**, *109*, 6366−6374.

(13) Shiflett, M. B.; Niehaus, A. M. S.; Yokozeki, A. Separation of N_2O and CO_2 Using Room-Temperature Ionic Liquid [bmim][BF_4]. *J. Phys. Chem. B* **2011**, *115*, 3478−3487.

(14) van der Berg, J.; Zhu, W. D.; Gascon, J.; Moulijn, J. A.; Kapteijn, F. Separation and Permeation Characteristics of a DD3R Zeolite Membrane. *J. Membr. Sci.* **2008**, *316*, 35−45.

(15) Centi, G.; Generali, P.; dall'Olio, L.; Perathoner, S.; Rak, Z. Removal of N_2O from Industrial Gaseous Streams by Selective Adsorption over Metal-Exchanged Zeolites. *Ind. Eng. Chem. Res.* **2000**, *39*, 131−137.

(16) Park, K. S.; Ni, Z.; Côté, A. P.; Choi, J. Y.; Huang, R.; Uribe-Romo, F. J.; Chae, H. K.; O'Keeffe, M.; Yaghi, O. M. Exceptional Chemical and Thermal Stability of Zeolitic Imidazolate Frameworks. *Proc. Natl. Acad. Sci. U. S. A.* **2006**, *103*, 10186−10191.

(17) Gücüyener, C.; van der Bergh, J.; Gascon, J.; Kapteijn, F. Ethane/Ethene Separation Turned on Its Head: Selective Ethane Adsorption on the Metal-Organic Framework ZIF-7 through a Gate-Opening Mechanism. *J. Am. Chem. Soc.* **2010**, *132*, 17704−17706.

(18) van der Bergh, J.; Gücüyener, C.; Pidko, E. A.; Hensen, E. J. M.; Gascon, J.; Kapteijn, F. Understanding the Anomalous Alkane Selectivity of ZIF-7 in the Separation of Light Alkane/Alkene Mixtures. *Chem.—Eur. J.* **2011**, *17*, 8832−8840.

(19) Zhang, J.-P.; Chen, X.-M. Optimized Acetylene/Carbon Dioxide Sorption in a Dynamic Porous Crystal. *J. Am. Chem. Soc.* **2009**, *131*, 5516−5521.

(20) Zhao, P.; Lampronti, G. I.; Lloyd, G. O.; Suard, E.; Redfern, S. A. T. Direct Visualisation of Carbon Dioxide Adsorption in Gate-Opening Zeolitic Imidazolate Framework. *J. Mater. Chem. A* **2014**, *2*, 620−623.

(21) Serre, C.; Millange, F.; Thouvenot, C.; Noguès, M.; Marsolier, G.; Louër, D.; Férey, G. Very Large Breathing Effect in the First Nanoporous Chromium(III)-Based Solids: MIL-3 or $Cr^{III}(OH)\cdot\{O_2C-C_6H_4-CO_2\}\cdot\{HO_2C-C_6H_4-CO_2H\}_x\cdot H_2O_y$. *J. Am. Chem. Soc.* **2002**, *124*, 13519−13526.

(22) Chen, L.; Mowat, J. P. S.; Fairen-Jimenez, D.; Morrison, C. A.; Thompson, S. P.; Wright, P. A.; Düren, T. Elucidating the Breathing of the Metal-Organic Framework MIL-53(Sc) with ab Initio Molecular Dynamics Simulations and in Situ X-ray Power Diffraction Experiments. *J. Am. Chem. Soc.* **2013**, *135*, 15763−15773.

(23) Kresse, G. Ab Initio Molecular-Dynamics for Liquid-Metals. *J. Non-Cryst. Solid* **1995**, *193*, 222−229.

(24) Kresse, G.; Hafner, J. Ab Initio Molecular-Dynamics Simulation of the Liquid-Metal-Amorphous-Semiconductor Transition in Germanium. *Phys. Rev. B* **1994**, *49*, No. 14251.

(25) Kresse, G.; Furthmuller, J. Efficient Iterative Schemes for ab Initio Total-Energy Calculations Using a Plane-Wave Basis Set. *Phys. Rev. B* **1996**, *54*, No. 11169.

(26) Kresse, G.; Furthmuller, J. Efficiency of ab Initio Total Energy Calculations for Metals and Semiconductors Using a Plane-Wave Basis Set. *Comput. Mater. Sci.* **1996**, *6*, 15−50.

(27) Klimes, J.; Bowler, D. R.; Michaelides, A. Chemical Accuracy for the van der Waals Density Functional. *J. Phys.: Condens. Matter* **2010**, *22*, 022201.

(28) Klimes, J.; Bowler, D. R.; Michaelides, A. van der Waals Density Functionals Applied to Solids. *Phys. Rev. B* **2011**, *83*, No. 195131.

(29) Monkhorst, H. J.; Pack, J. D. Special Points for Brillouin-Zone Integrations. *Phys. Rev. B* **1976**, *13*, No. 5188.

(30) Park, K. S.; Ni, Z.; Côté, A. P.; Choi, J. Y.; Huang, R.; Uribe-Romo, F. J.; Chae, H. K.; O'Keeffe, M.; Yaghi, O. M. Exceptional Chemical and Thermal Stability of Zeolitic Imidazolate Frameworks. *Proc. Natl. Acad. Sci. U. S. A.* **2006**, *103*, 10186−10191.

(31) Møller, C.; Plesset, M. S. Note on an Approximation Treatment for Many-Electron Systems. *Phys. Rev.* **1934**, *46*, No. 618.

(32) Adler, T. B.; Knizia, G.; Werner, H.-J. A Simple and Efficient CCSD(T)-F12 Approximation. *J. Chem. Phys.* **2007**, *127*, No. 221106.

(33) Derner, H.-J.; Knizia, G.; Manby, F. R. Explicitly Correlated Coupled Cluster Methods with Pair-Specific Geminals. *Mol. Phys.* **2011**, *109*, 407−417.

(34) Werner, H.-J.; Knowles, P. J.; Knizia, G.; Manby, F. R.; Schütz, M.; et al. *MOLPRO*, Version 2012.1, A Package of ab Initio Programs; see http://www.molpro.net.

(35) Heßelmann, A.; Jansen, G.; Schütz, M. Density-Functional Theory-Symmetry-Adapted Intermolecular Perturbation Theory with Density Fitting: A New Efficient Method to Study Intermolecular Interaction Energies. *J. Chem. Phys.* **2005**, *122*, No. 014103.

(36) Aguado, S.; Bergeret, G.; Pera-Titus, M.; Moizan, V.; Nieto-Draghi, C.; Bats, N.; Farrusseng, D. Guest-Induced Gate-Opening of a Zeolite Imidazolate Framework. *New J. Chem.* **2011**, *35*, 546−550.

(37) Myers, A. L.; Prausnitz, J. M. Thermodynamics of Mixed-Gas Adsorption. *AIChE J.* **1965**, *11*, 121−127.

(38) Haldoupis, E.; Nair, S.; Sholl, D. S. Efficient Calculation of Diffusion Limitations in Metal Organic Framework Materials: A Tool for Identifying Materials for Kinetic Separations. *J. Am. Chem. Soc.* **2010**, *132*, 7528−7539.

(39) Rana, M. K.; Koh, H. S.; Hwang, J.; Siegel, D. J. Comparing van der Waals Density Functionals for CO_2 Adsorption in Metal Organic Framework. *J. Phys. Chem. C* **2012**, *116*, 16957−16968.
(40) Chen, D.-L.; Mandeltort, L.; Saidi, W. A.; Yates, J. T., Jr.; Cole, M. W.; Johnson, J. K. Is There a Difference in van der Waals Interactions between Rare Gas Atoms Adsorbed on Metallic and Semiconducting Single Walled Carbon Nanotubes? *Phys. Rev. Lett.* **2013**, *110*, No. 135503.
(41) Mandeltort, L.; Chen, D.-L.; Saidi, W. A.; Johnson, J. K.; Cole, M. W.; Yates, J. T., Jr. Experimental and Theoretical Comparison of Gas Desorption Energies on Metallic and Semiconducting Single Walled Carbon Nanotubes. *J. Am. Chem. Soc.* **2013**, *135*, 7768−7776.
(42) Vaidhyanathan, R.; Iremonger, S. S.; Shimizu, G. K. H.; Boyd, P. G.; Alavi, S.; Woo, T. K. Direct Observation and Quantification of CO_2 Binding Within an Amine-Functionalized Nanoporous Solids. *Science* **2010**, *330*, 650−653.
(43) Culp, J. T.; Chen, D.-L.; Liu, J.; Chirdon, D.; Goodman, A.; Johnson, J. K. Effect of Spin Crossover Induced Pore Contraction on CO_2-Host Interactions in the Porous Coordination Polymers Fe(Pyrazine)$M(CN)_4$ (M = Ni, Pt). *Eur. J. Inorg. Chem.* **2013**, 511−519.
(44) Krishna, R.; Long, J. R. Screening Metal-Organic Frameworks by Analysis of Transient Breakthrough of Gas Mixtures in a Fixed Bed Adsorber. *J. Phys. Chem. C* **2011**, *115*, 12941−12950.
(45) Bloch, E. D.; Queen, W. L.; Krishna, R.; Zadrozny, J. M.; Brown, C. M.; Long, J. R. Hydrocarbon Separations in a Metal-Organic Framework with Open Iron(II) Coordination Sites. *Science* **2012**, *335*, 1606−1610.
(46) Krishna, R. The Maxwell-Stefan Desorption of Mixture Diffusion in Nanoporous Crystalline Materials. *Microporous Mesoporous Mater.* **2014**, *185*, 30−50.
(47) Reyes, S. C.; Santiesteban, J. G.; Ni, Z.; Paur, C. S.; Kortunov, P.; Zengel, J.; Deckman, H. W. Separation of Carbon Dioxide From Nitrogen Utilizing Zeolitic Imidazolate Framework Materials. U.S. Patent 8,142,745, 2012.

Supporting Information accompanying

Utilizing the Gate-Opening Mechanism in ZIF-7 for Adsorption Discrimination between N_2O and CO_2

De-Li Chen,[†] Ningwei Wang,[†] Fang-Fang Wang,[†] Jianwu Xie,[†] Yijun Zhong,[†] Weidong Zhu,*[†] J. Karl Johnson,[‡,§] Rajamani Krishna,*[‖]

[†]Key Laboratory of the Ministry of Education for Advanced Catalysis Materials, Institute of Physical Chemistry, Zhejiang Normal University, 321004 Jinhua, China

[‡]Department of Chemical and Petroleum Engineering, University of Pittsburgh, Pittsburgh, Pennsylvania 15261, United States

[§]National Energy Technology Laboratory, Pittsburgh, Pennsylvania 15236, United States

[‖] Van't Hoff Institute for Molecular Science, University of Amsterdam, Science Park 904, 1098 XH Amsterdam, The Netherlands

I. Synthesis and Characterization of ZIF-7

Benzimidazole ($C_7H_6N_2$, 98.5%) and N,N-dimethylformamide (DMF, AR) were purchased from Jingchun Industry Co., Ltd, Shanghai, China, and zinc nitrate hexahydrate [$Zn(NO_3)_2 \cdot 6H_2O$, AR] and methanol (AR) were supplied by Sinopharm Chemical Reagent Co., Ltd, Shanghai, China. All chemicals were used without further purification. The synthesis of ZIF-7 crystals was carried out according to the procedure reported by Gücüyener *et al*.[1]

The XRD pattern of the synthesized ZIF-7 is shown in Figure S1. The SEM image of the synthesized ZIF-7 shown in Figure S2 reveals that ZIF-7 has a rhombic dodecahedral shape with 12 exposed {110} faces and a hexagonal cross-section, and the size is up to 20 μm.

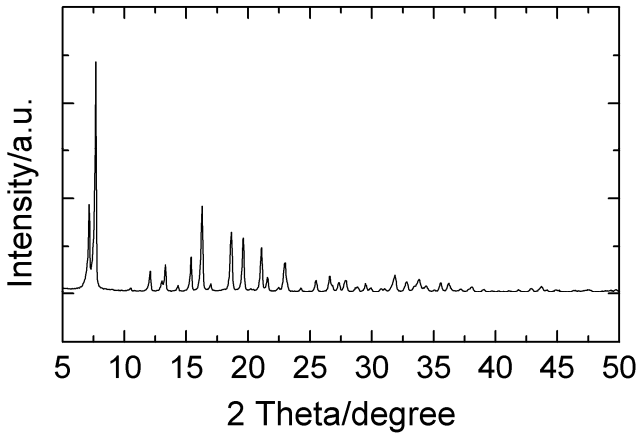

Figure S1. XRD pattern of the synthesized ZIF-7.

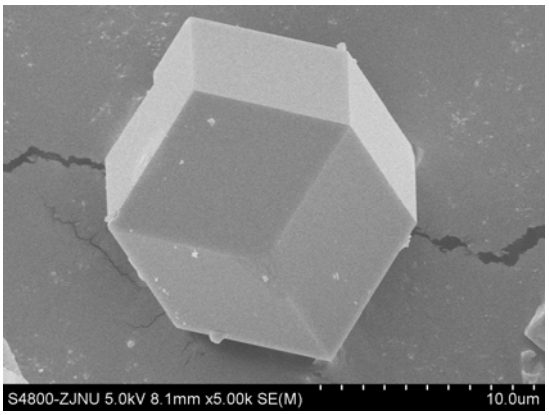

Figure S2. SEM micrograph of ZIF-7 with a rhombic dodecahedral shape.

II. Dual-site Langmuir-Freundlich (DLF) Isotherm Model

Table S1. Estimated parameter values for the fitting of the adsorption and desorption data of CO_2 and N_2O in ZIF-7 at 298 K by the dual-site Langmuir-Freundlich model

	Site A			Site B		
	$q_{A,sat}$ (mmol/g)	b_A ($Pa^{-\nu_A}$)	ν_A (dimensionless)	$q_{B,sat}$ (mmol/g)	b_B ($Pa^{-\nu_B}$)	ν_B (dimensionless)
N_2O, adsorption branch	1.88	5.22×10^{-83}	17.8	4.7	1.19×10^{-5}	0.8
N_2O, desorption branch	1.9	5.65×10^{-96}	21	15	3.57×10^{-4}	0.4
CO_2, adsorption branch	1.9	4.37×10^{-81}	16.9	3	1.2×10^{-5}	0.8
CO_2, desorption branch	1.8	1.24×10^{-121}	25.9	35	7.74×10^{-5}	0.45

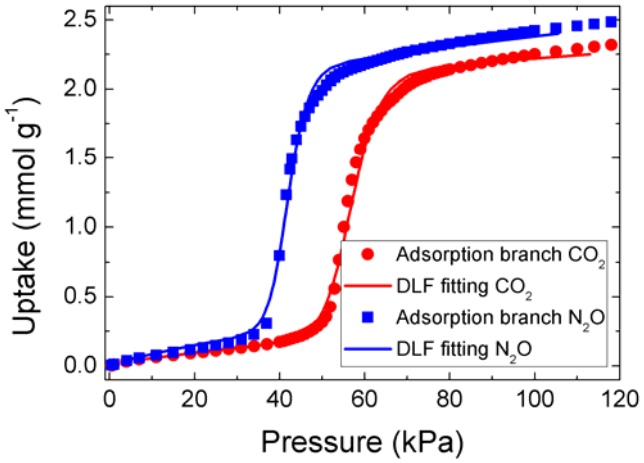

Figure S3. Comparison of the measured N_2O and CO_2 adsorption isotherms (symbols) and the fitted adsorption isotherms (lines) at 298 K.

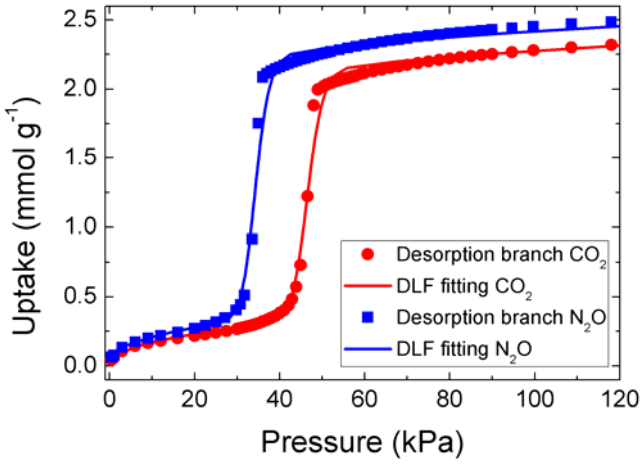

Figure S4. Comparison of the measured N_2O and CO_2 desorption isotherms (symbols) and the fitted desorption isotherms (dashed lines) at 298 K.

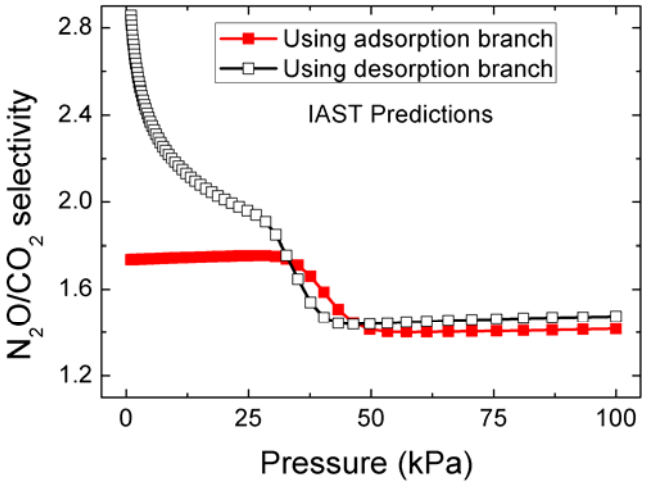

Figure S5. IAST adsorption/desorption selectivity for N_2O over CO_2 (50:50 mixture) in ZIF-7 at 298 K as a function of the total gas phase pressure.

III. Details of Theoretical Calculations

Density functional theory calculations were performed in Vienna ab initio simulation package.[2-5] The van der Waals density functional, specifically using the vdW-DF2,[6] was used to reproduce the van der Waals energy between the gas molecules and framework. The Brillouin zone was sampled using Monkhorst-Pack grids[7] of 1×1×1 for all of the calculations, where a planewave energy cutoff of 400 eV was employed. Note that in this study the experimentally measured unit cell (a = b = 22.989 Å, c = 15.763 Å)[8] was fixed while all the atoms on the framework of ZIF-7 were fully relaxed using vdW-DF2 method.

The potential energy (also denoted as adsorption energy) of gas molecule in ZIF-7 at different sites was calculated as $E_{pot} = E_{gas/ZIF\text{-}7} - E_{ZIF\text{-}7} - E_{gas}$, where $E_{gas/ZIF\text{-}7}$, $E_{ZIF\text{-}7}$, and E_{gas} represent energies of fully relaxed structure of gas/ZIF-7, pure ZIF-7, and isolated gas molecule, respectively. The potential energy curves of CO_2, N_2O with NNO orientation, and N_2O with ONN orientation were plotted in Figure 2.

The pore sizes of pore-A and pore-B in ZIF-7 are simply described as the distance between a pair of opposite H atoms around the pores, as illustrated in Figure S6. The calculations show that the adsorption of the N_2O at the pore-A site greatly increases the size of pore-A from 4.8 to 5.7 Å, while the adsorption of the N_2O at the pore-B site (with a size of 6.2 Å) is almost unchanged. The adsorption of CO_2 changes the sizes of both pore-A and pore-B with the same magnitude as those of N_2O adsorption.

For evaluating the intermolecular interaction of $N_2O\cdots N_2O$ (or $CO_2\cdots CO_2$) linear configuration, Gaussian 09 package[9] was used. Two different configurations of $N_2O\cdots N_2O$, that is, symmetric NNO···ONN and NNO···NNO were considered. The MP2 method[10] together with basis set of aug-cc-pVTZ was employed for structural optimizations and then the obtained structures (Figure S7) were used for single point calculations using explicitly correlated coupled cluster singles and doubles with perturbative triples method [CCSD(T)-F12a][11,12] implemented in Molpro program.[13] The DFT-SAPT method[14] was also used for decomposition of the interaction energies between CO_2 (or N_2O) molecules. The decomposed energies can provide insights on the origin of the interaction energies and thus explain the differences between gas dimers, although the total interaction energies predicted using DFT-SAPT are consistently shifted to more repulsive interaction energies comparing to CCSD(T)-F12a data by 0.4-0.5 kJ/mol. The E_{int} (interaction energy), E_{ind} (induction energy), E_{disp} (dispersion energy), E_{el} (electrostatic energy), and E_{ex} (exchange energy) for OCO···OCO, NNO···ONN, and NNO···NNO are listed in Table S2.

Eguchi *et al.*[15] pointed that N_2O shares many similar physical properties with CO_2, including molecular size and quadrupole moment, *i.e.*, both of N_2O and CO_2 molecules have a kinetic diameter of 3.3 Å, and the quadrupole moment of CO_2 (-14.9×10^{-40} C m^2) is slightly larger than that of N_2O (-11.2×10^{-40} C m^2). Different from the nonpolar CO_2 molecule, N_2O has a small dipole moment of 0.167 Debye.[16] The atomic charges of N_2O were fitted using ChelpG method for both N_2O and CO_2 molecules at the level of MP2/aug-cc-pVDZ in this study and the calculations show that the nitrogen atom at the central site of N_2O molecule has a positive charge of 0.63 |e|, while the fitted charges for the other nitrogen atom and oxygen atom are -0.27 and -0.36 |e|, respectively, of which the population of the atomic charges for N_2O are the same for CO_2 but with slightly different magnitude, *i.e.*, 0.88 and -0.44 |e| for C and O, respectively. As shown in Table S2, the OCO···OCO has more repulsive E_{el} (0.9 kJ/mol) than that of NNO···ONN (0.3 kJ/mol), while

NNO···NNO has an even smaller value of 0.2 kJ/mol because of its attractive dipole-dipole interaction (included in the E_{el}). Therefore, we conclude that it is the qudrupole-quadrupole term dominating the electrostatic energy, leading to a more repulsive electrostatic energy for CO_2 dimer because of its relatively larger quadrupole moment, while the small dipole moment of N_2O has a much smaller effect on the intermolecular interaction.

Table S2. Decomposition of intermolecular interaction energies computed from DFT-SAPT for OCO···OCO, NNO···ONN, and NNO···NNO, where E_{int}, E_{ind}, E_{disp}, E_{el}, and E_{ex} (in kJ/mol) represent the total interaction energy, induction energy, dispersion energy, electrostatic energy, and exchange energy, respectively

	E_{int}	E_{ind}	E_{disp}	E_{el}	E_{ex}
	kJ/mol				
OCO···OCO	0.4	-0.1	-2.8	0.9	2.4
NNO···ONN	-1.0	-0.1	-2.9	0.3	1.7
NNO···NNO	-0.3	-0.1	-3.4	0.2	3.0

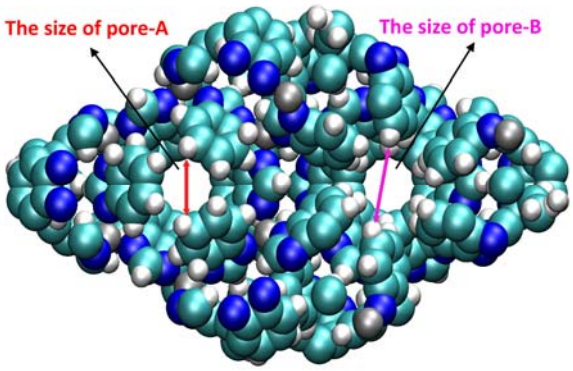

Figure S6. Schematic representations for the sizes of pore-A and pore-B along the *z*-axis of the ZIF-7 crystal structure.

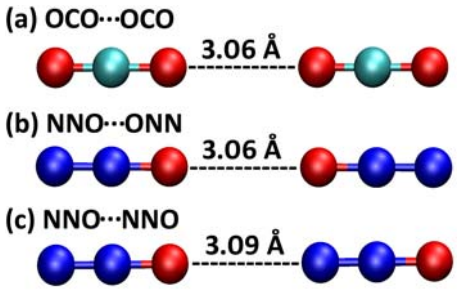

Figure S7. Optimized intermolecular distances of the CO_2 dimer and two different N_2O dimers.

IV. Breakthrough Experiments and Simulations

The setup consists of three sections: a gas mixing and flow control section, a breakthrough column, and an analysis section. A flow-sheet diagram of the setup is shown in Figure S8. The mixing section contains a total of four mass flow controllers (MFC1-4). The two adsorbing gases are introduced into the mixing section via two mass flow controllers (MFC3 and MFC4) with an

operation range of 0-20 mL (STP)·min^{-1} (STP: 273 K & 1 atm). The two adsorbing gases can be mixed with He from MFC2 [0-200 mL (STP)/min]. The desorption gas flow is controlled with MFC1 [0-200 mL (STP)/min].

The breakthrough column was installed inside the ceramic oven, which was located inside the convection oven. The external diameter of the column was 6.35 mm with a length of 15 cm and the inner diameter was 4.65 mm. The pressure drop across the column was monitored by the differential pressure (dp) sensor. The pressure in the outlet of the column was regulated with the back pressure controller (BPC1). The gas flow sent to the analysis section could be adjusted with the needle valve (V4). Selection valve V2 allowed either the feed or purge gas pass the column, and selection valve V3 allowed either the feed or the flow from the outlet of the column to be sent to the analysis section.

The mass spectrometer (Pfeiffer Vacuum OmniStar GSD 320) in the analysis section was used to monitor the component concentrations continuously. However, for N_2O/CO_2 mixtures, most of the intense m/e peaks overlap and thus the composition cannot be identified by the mass spectrometer. In order to determine the breakthrough and desorption profiles of the mixture compositions, the isotope gas $^{13}CO_2$, provided by Beijing Mingnike Analytical Instrument Center (^{13}C > 99% and ^{18}O < 1%), was used. The N_2O was supplied by Beijing Praxair Application Gas Co., Ltd (>99.99%).

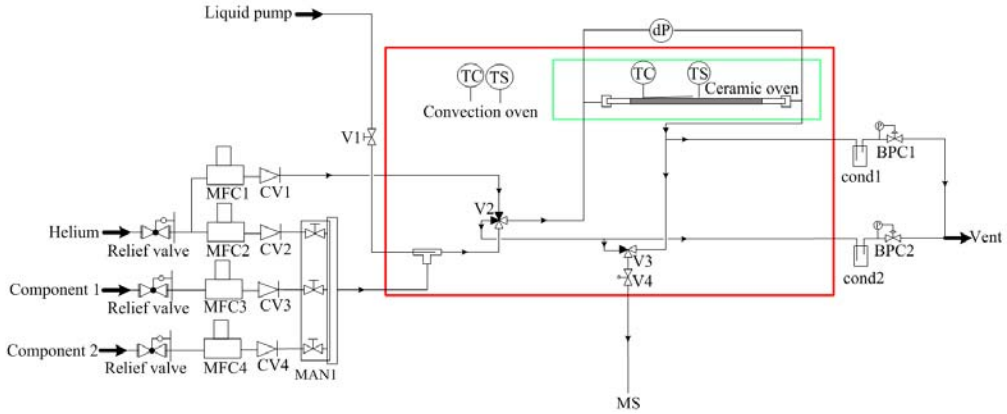

Figure S8. Flow-sheet diagram of the breakthrough setup.

The breakthrough experiments were performed at a total pressure of 200 kPa at 298 K by switching the flow to the column from He to N_2O and $^{13}CO_2$ in He. After the breakthrough curves reached the equilibrium, the mixture feed flow of N_2O and $^{13}CO_2$ in He was switched back to the He flow with a rate of 20 mL (STP)/min and the desorption curves were recorded (see Figure S9 for the desorption curves).

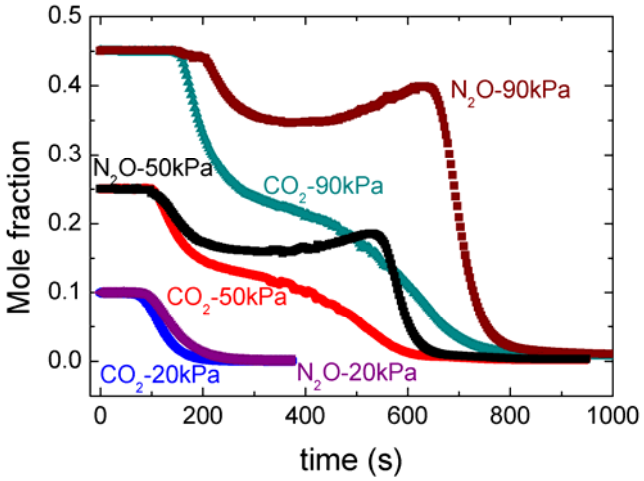

Figure S9. Measured mole fractions of N_2O and CO_2 in the outlet of the column from the three desorption experiments at 298 K as a function of time, where both N_2O and CO_2 inlet partial pressures for the breakthrough experiments are 20, 50, and 90 kPa, respectively.

The breakthrough simulations (see next section for simulation details) were performed and compared to the results of Exp-1, Exp-2, and Exp-3. The comparison of Exp-2 and simulation results with both CO_2 and N_2O inlet partial pressures of 50 kPa is shown in Figure 4 in the paper, herein, only the comparisons between Exp-1 (and Exp-3) and simulation results with both CO_2 and N_2O inlet partial pressures of 50 and 90 kPa are presented (see Figures S10 and 11). Note that for the breakthrough simulations taking into account of the intra-crystalline diffusion, constant Fick diffusivities $Đ_i/r_c^2$ = 0.005 for both N_2O and CO_2 are used, where r_c is the radius of the crystallites packed in the breakthrough column.

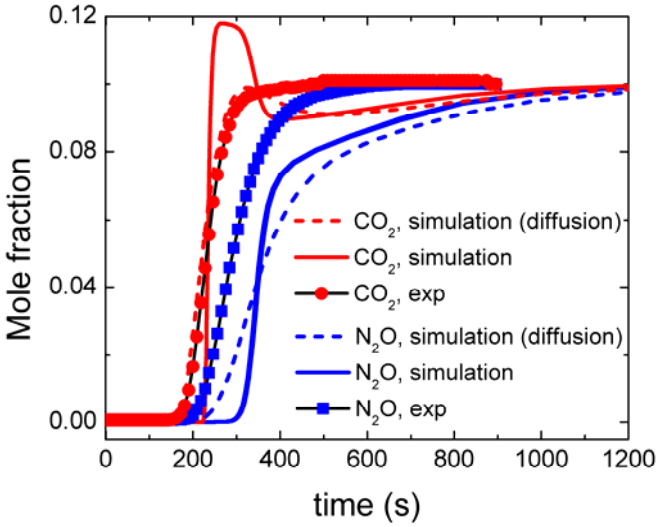

Figure S10. Comparison of Exp-1 and simulation results with both CO_2 and N_2O inlet partial pressures of 20 kPa. The symbols represent experimental data; solid lines and dashed lines are for simulation data without and with the consideration of intra-crystalline diffusion, respectively.

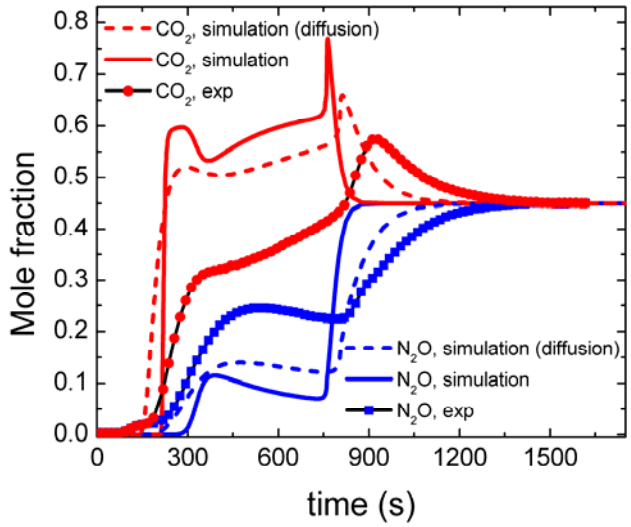

Figure S11. Comparison of Exp-3 and simulation results with both CO_2 and N_2O inlet partial pressures of 90 kPa. The symbols represent experimental data; solid lines and dashed lines are for simulation data without and with the consideration of intra-crystalline diffusion, respectively.

The CO_2/N_2O and N_2O/CO_2 ratio in the outlet of the breakthrough column for both adsorption and desorption cycles as a function of time, based on the simulation, are presented in Figure S12.

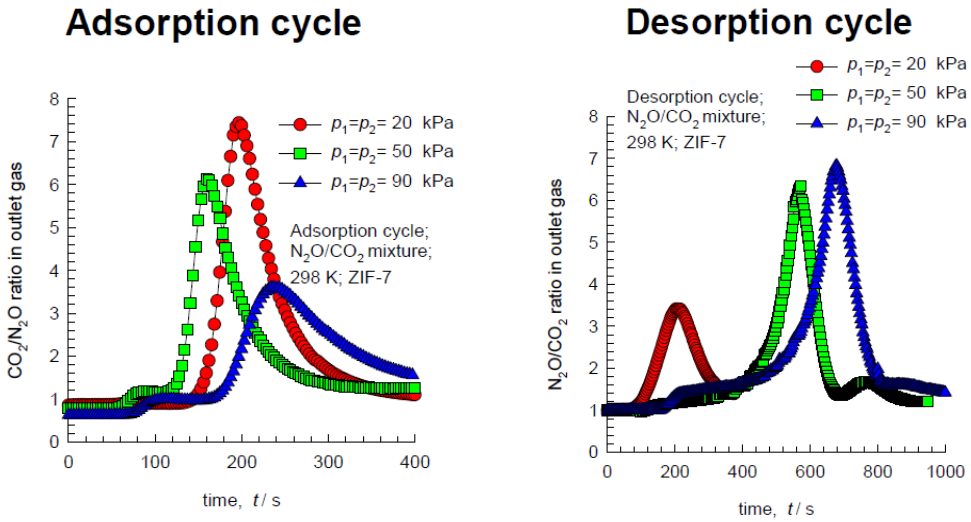

Figure S12. (a) CO_2/N_2O and (b) N_2O/CO_2 ratios in the outlet from the breakthrough column from adsorption and desorption simulations.

V. Simulation Methodology for Transient Breakthrough in Fixed Bed Adsorbers

Fixed beds, packed with crystals of nanoporous materials, are commonly used for separation of mixtures (see a schematic representation in Figure S13); such adsorbers are commonly operated in a transient mode, and the compositions of the gas phase, and within the crystals, vary with position and time. Experimental data on the transient breakthrough of mixtures across fixed beds are commonly used to evaluate and compare the separation performance of zeolites and MOFs.[1,17-20] For a given separation task, transient breakthroughs

provide more a realistic evaluation of the efficacy of a material, as they reflect the combined influence of adsorption selectivity and adsorption capacity.[20,21]

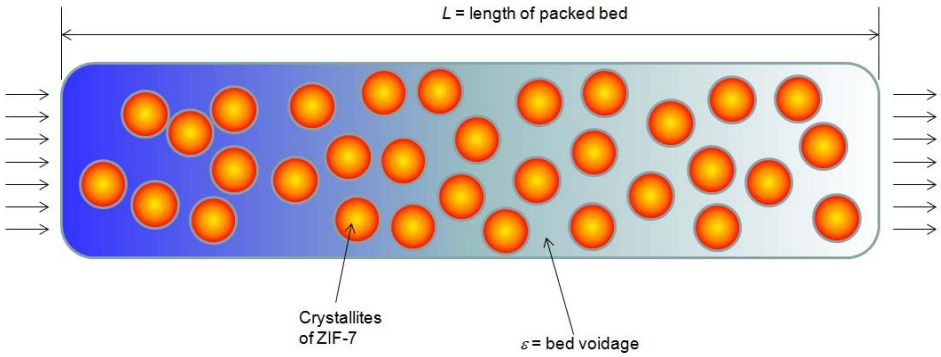

Figure S13. Schematic diagram of a packed bed adsorber.

Furthermore, transient breakthroughs are influenced by both mixture adsorption equilibrium and intra-crystalline diffusion. In order to determine the extent of the relative importance of adsorption and diffusion in determining the separation performance we perform transient breakthrough simulations, and compare these with experimental data. We describe below the simulation methodology used to perform transient breakthrough calculations.

Assuming plug flow of an *n*-component gas mixture through a fixed bed maintained under isothermal conditions, the partial pressures in the gas phase at any position and instant of time are obtained by solving the following set of partial differential equations for each of the species *i* in the gas mixture.[20]

$$\frac{1}{RT}\frac{\partial p_i(t,z)}{\partial t} = -\frac{1}{RT}\frac{\partial \left(v(t,z)p_i(t,z)\right)}{\partial z} - \frac{\left(1-\varepsilon\right)}{\varepsilon}\rho\frac{\partial \bar{q}_i(t,z)}{\partial t}; \quad i=1,2,...n \qquad (1)$$

In equation (1), t is the time, z is the distance along the adsorber, ρ is the framework density, ε is the bed voidage, v is the interstitial gas velocity, and $\bar{q}_i(t,z)$ is the *spatially averaged* molar loading within the crystallites of radius r_c, monitored at position z and at time t.

At any time t, during the transient approach to thermodynamic equilibrium, the spatially averaged molar loading within the crystallite r_c is obtained by integration of the radial loading profile

$$\bar{q}_i(t) = \frac{3}{r_c^3}\int_0^{r_c} q_i(r,t)r^2 dr \qquad (2)$$

For transient unary uptake within a crystal at any position and time with the fixed bed, the radial distribution of molar loadings, q_i, within a spherical crystallite of radius r_c, is obtained from a solution of a set of differential equations describing the uptake

$$\frac{\partial q_i(r,t)}{\partial t} = -\frac{1}{\rho}\frac{1}{r^2}\frac{\partial}{\partial r}\left(r^2 N_i\right) \qquad (3)$$

The molar flux N_i of component i is described by the simplified version of the Maxwell-Stefan equations in which both correlation effects and thermodynamic coupling effects are considered to be of negligible importance.[20]

$$N_i = -\rho Đ_i \frac{\partial q_i}{\partial r} \tag{4}$$

Summing equation (2) over all n species in the mixture allows calculation of the *total average* molar loading of the mixture within the crystallite

$$\overline{q}_t(t,z) = \sum_{i=1}^{n} \overline{q}_i(t,z) \tag{5}$$

The *interstitial* gas velocity is related to the *superficial* gas velocity by

$$v = \frac{u}{\varepsilon} \tag{6}$$

In industrial practice, the most common operation is to use a step-wise input of mixtures to be separated into an adsorber bed that is initially free of adsorbates, *i.e.,* we have the initial condition

$$t = 0; \quad q_i(0,z) = 0 \tag{7}$$

At time t = 0, the inlet to the adsorber, z = 0, is subjected to a step input of the n-component gas mixture and this step input is maintained till the end of the adsorption cycle when steady-state conditions are reached.

$$t \geq 0; \quad p_i(0,t) = p_{i0}; \quad u(0,t) = u_0 \tag{8}$$

where u_0 is the superficial gas velocity at the inlet to the adsorber.

Further details of the numerical procedures used in this work are provided by Krishna and co-workers.[22-24]

If the value of $\frac{Đ_i}{r_c^2}$ is large enough to ensure that intra-crystalline gradients are absent and the entire crystallite particle can be considered to be in thermodynamic equilibrium with the surrounding bulk gas phase at that time t, and position z of the adsorber

$$\overline{q}_i(t,z) = q_i(t,z) \tag{9}$$

The molar loadings at the *outer surface* of the crystallites, *i.e.,* at $r = r_c$, are calculated on the basis of adsorption equilibrium with the bulk gas phase partial pressures p_i at that position z and time t. The adsorption equilibrium can be calculated on the basis of the IAST.

When matching experimental data on breakthroughs, the parameter values used correspond to those relevant to the experiments being simulated. Two types of breakthrough simulations were performed for each experimental run: (a) including diffusional limitations with assumed

values of $Đ_i/r_c^2$ for matching with experimental breakthroughs and (b) assuming negligible diffusional limitations and invoking equation (9).

VI. Accuracy of IAST Prediction

To estimate the reliability of IAST predictions of gas mixtures on ZIF-7, we also computed the adsorption loading using the breakthrough data discussed above under various conditions.

We develop here the material balance equations for analyzing the transient breakthroughs of N_2O/CO_2/He mixture in a tube packed with ZIF-7 crystallites. The analysis presented below is essentially that of Pirngruber et al.[25] From the crystallographic data, the framework or "grain" density of ZIF-7, ρ = 1241 kg m^{-3}.

Let us consider a tube of inside diameter, *d*, with a length *L* packed with crystallites of ZIF-7. The cross-sectional area of the tube, *A*, is

$$A = \frac{\pi}{4} d^2 \tag{10}$$

The volume of the empty tube, *V*, is

$$V = AL \tag{11}$$

Let m_{ads} represents the mass of adsorbent ZIF-7 packed into the tube. The volume occupied by the adsorbent crystalline material, V_{ads}, is

$$V_{ads} = \frac{m_{ads}}{\rho} \tag{12}$$

If we denote the voidage of packed bed as ε, we also have the relationship

$$V_{ads} = (1-\varepsilon)V \tag{13}$$

Equation (13) allows us to determine the packed bed voidage ε for use in the breakthrough simulations that are also carried out.

In the breakthrough experiments, the volumetric flow rate of inert gas He is maintained constant at a value Q_{He}.

The experiments are carried out for a total period of time, t_{ss}, till the steady-state is reached. A material balance for the time interval t = 0 - t_{ss}, allows us to determine the component loadings q_i

$$(q_i - q_{i0})m_{ads} = c_t Q_{He} \int_0^{t_{ss}} \left(\frac{y_{i,inlet}}{y_{He,inlet}} - \frac{y_{i,exit}}{\sum_{i=1}^{2}(1-y_{i,exit})} \right) dt + (c_t y_{i,exit})(V_{ads} - AL) \tag{14}$$

We assume that the initial loadings in ZIF-7 are q_{i0}. In our "adsorption" experiments q_{i0} = 0. The second term on the right hand side represents the "dead volume" correction. This correction is properly accounted for in our calculations.

The integral in equation (14) can be determined numerically from the breakthrough experimental data. We used numerical quadrature formula, implemented in Excel for the calculations.

The computed N_2O and CO_2 loadings at equilibrium in ZIF-7 pellets under different conditions, estimated from breakthrough experiments, are plotted in Figure S14. The IAST predicted loadings for the two components (both adsorption and desorption cycles) are also plotted for comparison. Overall, we can see that that there is a reasonable agreement of adsorption data between experiments and those from IAST predictions, only the trend of CO_2 loading estimated from experiments is different from IAST prediction when the total gas phase pressure increases from 100 to 180 kPa. This reasonable agreement between experiments and IAST predictions indicate that the breakthrough simulations as well as the adsorption selectivity predicted from IAST are reasonably accurate.

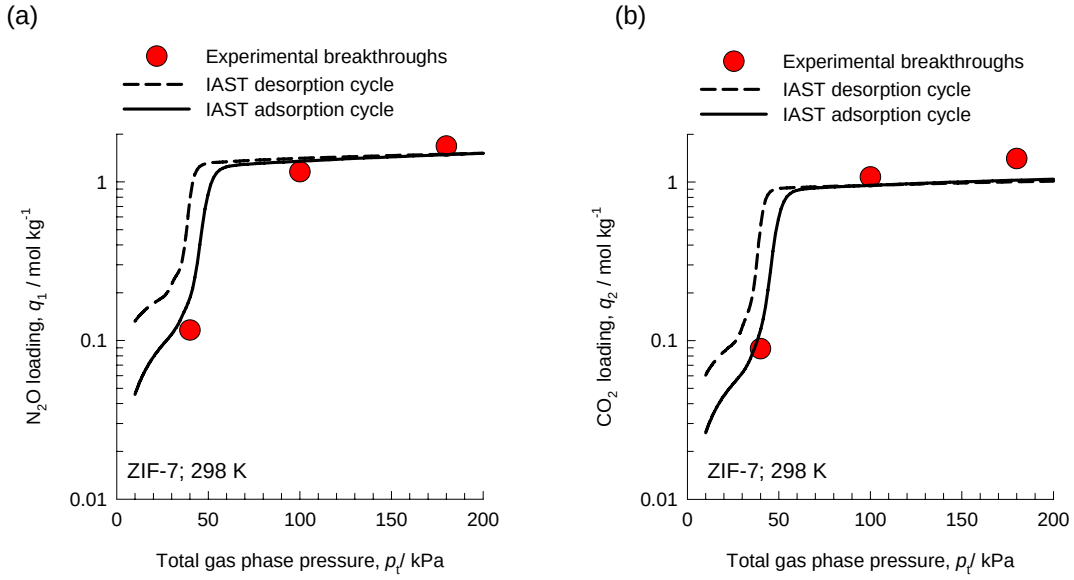

Figure S14. Comparison of (a) N_2O and (b) CO_2 adsorption loadings estimated from breakthrough experiments and IAST simulations.

VII. $N_2O/CO_2/N_2$ Breakthrough Simulations

In a US patent awarded to Exxon, Reyes et al.[26] present experimental isotherms for CO_2 and N_2 that suggest the strong potential for use of ZIF-7 in capture of CO_2 from flue gas mixtures. The experimental isotherm data of Reyes et al. for N_2 could be fitted with a single-site Langmuir model, and the fit parameters are provided in Table S3. Using this isotherm information, in combination with experimental data in this study on pure component isotherm fits of the adsorption cycle, for N_2O and CO_2 in ZIF-7 at 298 K, we examined the potential of separation of a ternary 1:1:2 $N_2O/CO_2/N_2$ mixture in a fixed bed operating at a total pressure of 100 kPa. The transient breakthroughs are shown in Figure S15, which clearly confirms the potential of ZIF-7 for use in separation of both N_2O/N_2 and CO_2/N_2 mixtures.

Table S3. Single-site Langmuir fit parameters for N_2 in ZIF-7 at 298 K obtained from the experimental data in the US patent awarded to Exxon[17]

	$q_{A,sat}$ (mmol/g)	b_A (Pa^{-1})
N_2	0.3	2×10^{-6}

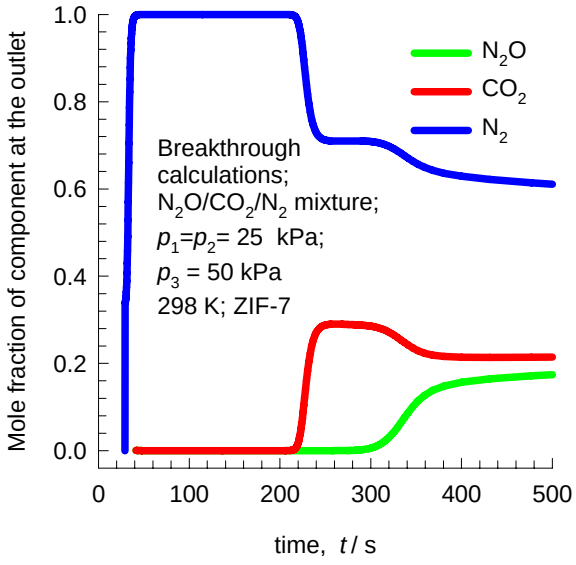

Figure S15. Simulated breakthrough curves of 1:1:2 $N_2O/CO_2/N_2$ ternary mixture in ZIF-7 at 298 K under a total pressure of 100 kPa.

Notations

A	cross-sectional area of the breakthrough column, m^2
b_A	dual-Langmuir-Freundlich constant for species *i* at adsorption site A, $Pa^{-\nu_i}$
b_B	dual-Langmuir-Freundlich constant for species *i* at adsorption site B, $Pa^{-\nu_i}$
c_i	molar concentration of species *i* in gas mixture, mol m^{-3}
c_{i0}	molar concentration of species *i* in gas mixture at the inlet of the adsorber, mol m^{-3}
d	inside diameter of the breakthrough column, m
$Đ_i$	Maxwell-Stefan diffusivity, m^2 s^{-1}
L	length of the breakthrough column, m
m_{ads}	mass of the adsorbent packed into the breakthrough column, kg
n	number of species in the mixture, dimensionless
N_i	molar flux of species *i*, mol m^{-2} s^{-1}
p_i	partial pressure of species *i* in mixture, Pa
p_t	total system pressure, Pa
q_i	component molar loading of species *i*, mol kg^{-1}
q_{i0}	initial component molar loading of species *i*, mol kg^{-1}
$q_{i,sat}$	saturation loading of species *i*, mol kg^{-1}
q_t	total molar loading in mixture, mol kg^{-1}
$q_{sat,A}$	saturation loading of site A, mol kg^{-1}
$q_{sat,B}$	saturation loading of site B, mol kg^{-1}
$\bar{q}_i(t)$	*spatially averaged* component molar loading of species *i*, mol kg^{-1}
Q_{He}	volumetric flow rate of inert gas He, m^3 s^{-1}
r_c	radius of crystallite, m
R	gas constant, 8.314 J mol^{-1} K^{-1}
t	time, s
t_{ss}	total period of time till the steady-state is reached, s
T	absolute temperature, K
u	superficial gas velocity in the packed bed, m s^{-1}
v	interstitial gas velocity in the packed bed, m s^{-1}
V	volume of the empty breakthrough column, m^3
V_{ads}	volume occupied by the adsorbent in the breakthrough column, m^3
y_i	mole fraction of component *i* in bulk vapor phase, dimensionless

Greek letters

ε	voidage of packed bed, dimensionless
ν	exponent in dual-Langmuir-Freundlich isotherm, dimensionless
ρ	framework density, kg m^{-3}

Subscripts

i	referring to component *i*
A	referring to site A
B	referring to site B
t	referring to total mixture

References

1. Gücüyener, C.; Van der Bergh, J.; Gascon, J.; Kapteijn, F. Ethane/Ethene Separation Turned on Its Head: Selective Ethane Adsorption on the Metal-Organic Framework ZIF-7 through a Gate-Opening Mechanism. *J. Am. Chem. Soc.*, **2010**, *132*, 17704-17706.
2. Kresse, G. Ab Initio Molecular-Dynamics for Liquid-Metals. *J. Non-Cryst. Solid*, **1995**, *193*, 222-229.
3. Kresse, G.; Hafner, J. Ab Initio Molecular-Dynamics Simulation of the Liquid-Metal-Amorphous-Semiconductor Transition in Germanium. *Phys. Rev. B*, **1994**, *49*, 14251.
4. Kresse, G.; Furthmuller, J. Efficient Iterative Schemes for ab Initio Total-Energy Calculations Using a Plane-Wave Basis Set. *Phys. Rev. B*, **1996**, *54*, 11169.
5. Kresse, G.; Furthmuller, J. Efficiency of ab Initio Total Energy Calculations for Metals and Semiconductors Using a Plane-Wave Basis Set. *Comput. Mater. Sci.*, **1996**, *6*, 15-50.
6. Lee, K.; Murray, É. D.; Kong, J.; Lundqvist, B. L.; Langreth, D. C. Higher-Accuracy van der Waals Density Functional. *Phys. Rev. B*, **2010**, *82*, 081101.
7. Monkhorst, H. J.; Pack, J. D. Special Points for Brillouin-Zone Integrations. *Phys. Rev. B*, **1976**, *13*, 5188.
8. Park, K. S.; Ni, Z.; Côté, A. P.; Choi, J. Y.; Huang, R.; Uribe-Romo, F. J.; Chae, H. K.; O'Keeffe, M.; Yaghi, O. M. Exceptional Chemical and Thermal Stability of Zeolitic Imidazolate Frameworks. *Proc. Natl. Acad. Sci. USA*, **2006**, *103*, 10186-10191.
9. Frisch, M. J.; Trucks, G. W.; Schlegel, H. B.; Scuseria, G. E.; Robb, M. A.; Cheeseman, J. R.; Scalmani, G.; Barone, V.; Mennucci, B.; Petersson, G. A.; Nakatsuji, H.; Caricato, M.; Li, X.; Hratchian, H. P.; Izmaylov, A. F.; Bloino, J.; Zheng, G.; Sonnenberg, J. L.; Hada, M.; Ehara, M.; Toyota, K,; Fukuda, R.; Hasegawa, J.; Ishida, M.; Nakajima, T.; Honda, Y.; Kitao, O.; Nakai, H.; Vreven, T.; Montgomery, J. A., Jr.; Peralta, J. E.; Ogliaro, F.; Bearpark, M.; Heyd, J. J.; Brothers, E.; Kudin, K. N.; Staroverov, V. N.; Kobayashi, R.; Normand, J.; Raghavachari, K.; Rendell, A.; Burant, J. C.; Iyengar, S. S.; Tomasi, J.; Cossi, M.; Rega, N.; Millam, N. J.; Klene, M.; Knox, J. E.; Cross, J. B.; Bakken, V.; Adamo, C.; Jaramillo, J.; Gomperts, R.; Stratmann, R. E.; Yazyev, O.; Austin, A. J.; Cammi, R.; Pomelli, C.; Ochterski, J. W.; Martin, R. L.; Morokuma, K.; Zakrzewski, V. G.; Voth, G. A.; Salvador, P.; Dannenberg, J. J.; Dapprich, S.; Daniels, A. D.; Farkas, Ö.; Foresman, J. B.; Ortiz, J. V.; Cioslowski, J.; Fox, D. J. Gaussian 09, Revision D.01, Gaussian, Inc., Wallingford CT, **2009**.
10. Møller, C.; Plesset, M. S. Note on an Approximation Treatment for Many-Electron Systems. *Phys. Rev.*, **1934**, *46*, 618.
11. Adler, T. B.; Knizia, G.; Werner, H.-J. A Simple and Efficient CCSD(T)-F12 Approximation. *J. Chem. Phys.*, **2007**, *127*, 221106.
12. Werner, H.-J.; Knizia, G.; Manby, F. R. Explicitly Correlated Coupled Cluster Methods with Pair-Specific Geminals. *Mol. Phys.*, **2011**, *109*, 407-417.
13. MOLPRO, Version 2012.1, A Package of ab Initio Programs, Werner, H.-J.; Knowles, P. J.; Knizia, G.; Manby, F. R.; Schütz, M. and others, see http://www.molpro.net.
14. Heßelmann, A.; Jansen, G.; Schütz, M. Density-Functional Theory-Symmetry-Adapted Intermolecular Perturbation Theory with Density Fitting: A New Efficient Method to Study Intermolecular Interaction Energies. *J. Chem. Phys.*, **2005**, *122*, 014103.
15. Eguchi, R.; Uchida, S.; Mizuno, N. Inverse and High CO_2/C_2H_2 Sorption Selectivity in

Flexible Organic-Inorganic Ionic Crystals. *Angew. Chem. Int. Ed.*, **2012**, *51*, 1635-1639.

16. Nelson, R. D., Jr.; Lide, D. R., Jr.; Maryott, A. A. Selected Values of Electric Dipole Moments for Molecules in the Gas Phase. NSRDS-NBS10, **1967**.
17. Bloch, E. D.; Queen, W. L.; Krishna, R.; Zadrozny, J. M.; Brown, C. M.; Long, J. R. Hydrocarbon Separations in a Metal-Organic Framework with Open Iron(II) Coordination Sites. *Science*, **2012**, *335*, 1606-1610.
18. Herm, Z. R.; Wiers, B. M.; van Baten, J. M.; Hudson, M. R.; Zajdel, P.; Brown, C. M.; Maschiocchi, N.; Krishna, R.; Long, J. R. Separation of Hexane Isomers in a Metal-Organic Framework with Triangular Channels. *Science*, **2013**, *340*, 960-964.
19. Yang, J.; Krishna, R.; Li, J.; Li, J. Experiments and Simulations on Separating a CO_2/CH_4 Mixture Using K-KFI at Low and High Pressures. *Microporous Mesoporous Mat.*, **2014**, *184*, 21-27.
20. Krishna, R. The Maxwell-Stefan Desorption of Mixture Diffusion in Nanoporous Crystalline Materials. *Microporous Mesoporous Mat.*, **2014**, *185*, 30-50.
21. Krishna, R.; Long, J. R. Screening Metal-Organic Frameworks by Analysis of Transient Breakthrough of Gas Mixtures in a Fixed Bed Adsorber. *J. Phys. Chem. C*, **2011**, *115*, 12941-12950.
22. Krishna, R.; Baur, R. Modeling Issues in Zeolite Based Separation Processes. *Sep. Purif. Technol.*, **2003**, *33*, 213-254.
23. Krishna, R.; Baur, R. Diffusion, Adsorption and Reaction in Zeolites: Modelling and Numerical Issues, http://www.science.uva.nl/research/cr/zeolite/, University of Amsterdam, Amsterdam, 11 November **2003**.
24. He, Y. B.; Krishna, R.; Chen, B. L. Metal-Organic Framework with Potential for Energy-Efficient Adsorptive Separation of Light Hydrocarbons. *Energy Environ. Sci.*, **2012**, *5*, 9107-9120.
25. Pirngruber, G. D.; Hamon, L.; Bourrelly, S.; Llewellyn, P. L.; Lenoir, E.; Guillerm, V.; Serre, C.; Devic, T. A Method for Screening the Potential of MOFs as CO_2 Adsorbents in Pressure Swing Adsorption Processes. *Chemsuschem*, **2012**, *5*,762-776.
26. Reyes, S. C.; Santiesteban, J. G.; Ni, Z.; Paur, C. S.; Kortunov, P.; Zengel, J.; Deckman, H. W. Separation of Carbon Dioxide From Nitrogen Utilizing Zeolitic Imidazolate Framework Materials. U.S. Patent 8,142,745, **2012**.